Efficient Zygotic Genome Editing via RAD51-Enhanced Interhomolog Repair

Jonathan J. Wilde[1,3], Tomomi Aida[1,3], Martin Wienisch[1], Qiangge Zhang[1], Peimin Qi[1], and Guoping Feng[1,2*]

Affiliations:
[1]McGovern Institute for Brain Research, Department of Brain and Cognitive Sciences, Massachusetts Institute of Technology (MIT), Cambridge, Massachusetts 02139, USA

[2]Stanley Center for Psychiatric Research, Broad Institute of MIT and Harvard, Cambridge, Massachusetts 02142, USA

[3]These authors contributed equally to this work.

***E-mail:** fengg@mit.edu

Recent advances in genome editing have greatly improved knock-in (KI) efficiency[1-9]. Searching for factors to further improve KI efficiency for therapeutic use and generation of non-human primate (NHP) models, we found that the strand exchange protein RAD51 can significantly increase homozygous KI using CRISPR/Cas9 in mouse embryos through an interhomolog repair (IHR) mechanism. IHR is well-described in the context of meiosis[10], but only occurs at low frequencies in mitotic cells[11,12] and its existence in zygotes is controversial. Using a variety of approaches, we provide evidence for an endogenous IHR mechanism in zygotes that can be enhanced by RAD51. We show that this process can be harnessed for generating homozygous KI animals from wildtype zygotes based on exogenous donors and for converting heterozygous alleles into homozygous alleles without exogenous templates. Furthermore, we elucidate additional factors that contribute to zygotic IHR and identify a RAD51 mutant capable of insertion-deletion (indel)-free stimulation of IHR. Thus, our study provides conclusive evidence for the existence of zygotic IHR and demonstrates methods to enhance IHR for potential use in gene drives, gene therapy, and biotechnology.

We previously described a three-component CRISPR approach that employs Cas9 protein and chemically synthesized crRNA and tracrRNA for efficient KI of transgenes[1,2,9]. In addition, published work in rabbit embryos has shown significant enhancement of KI efficiency using RS-1, a chemical agonist of the homology-directed repair (HDR) pathway member RAD51[6]. We began by testing whether a combination of these techniques would promote high-efficiency knock-in of an autism-associated point mutation in *Chd2* (c.5051G>A; R1685H in human, R1684H in mouse; hereon referred to as *Chd2*^{R1684H}; **Fig. 1a**) using a single-stranded oligonucleotide donor (ssODN). Previous studies have shown that KI efficiency is affected by

70 the proximity of the Cas9 cut site and the insertion site[3], so we chose a guide positioned where
71 the cut site is directly adjacent to the desired G>A point mutation. Genotyping of mouse embryos
72 after pronuclear injection and *in vitro* culture with or without RS-1 (7.5μM) showed a high KI
73 efficiency at the targeted *Chd2* locus but revealed that RS-1 did not affect KI efficiency
74 (**Extended Data Fig. 1**). Although the known mechanisms of RAD51 function suggest it may
75 not promote knock-in with ssODNs, our previous success using exogenous Cas9 protein to
76 promote high-efficiency KI[1,9] and the fact that RS-1 effects are dosage-sensitive and
77 uncharacterized in mouse embryos[6] led us to hypothesize that the use of exogenous RAD51
78 protein in combination with three-component CRISPR could increase KI efficiency. We
79 performed both pronuclear (PNI) and cytoplasmic (CPI) injections of crRNA, tracrRNA, Cas9,
80 ssODN (30 ng/μL for PNI and 100 ng/μL for CPI), and RAD51 protein (10ng/μL) in mouse
81 zygotes and genotyped the resulting F_0 pups (example chromatograms in **Fig. 1b**). We observed
82 overall KI efficiencies of 78% (7/9) and 56% (5/9) for CPI and PNI, respectively (**Fig. 1c**).
83 Surprisingly, both CPI and PNI resulted in a homozygous KI efficiency of 56% (**Fig. 1d,** each
84 5/9). On-target editing was confirmed through the use of primers sitting outside of the ssODN
85 homology arms and breeding of homozygous animals with wildtype C57BL/6N mice confirmed
86 their homozygosity, as 36/36 F_1 progeny from 6 mating pairs genotyped as *Chd2*$^{R1684H/+}$ (**Fig.**
87 **1e**).
88 Since we did not initially generate *Chd2*^{R1684H} mice from injections lacking RAD51, we
89 performed additional injections to directly assess the ability of RAD51 to increase KI efficiency.
90 We did not observe significant differences in efficiency between CPI and PNI (**Fig. 1c,d** and
91 **Extended Data Table 1**), and therefore focused on our lab's standard PNI injection strategy for
92 the rest of this study. Zygotic injections into the paternal pronucleus were performed with and

93 without RAD51, embryos were cultured for two days before lysis and DNA purification, and
94 then nested PCR was performed. Sanger sequencing revealed that RAD51 increased overall KI
95 efficiency (**Fig. 2a**, **left,** p=0.034, one-tailed chi-square test) and strongly increased homozygous
96 KI efficiency (**Fig. 2a, middle**, includes mosaic embryos, p<0.0001, one-tailed chi-square test;
97 **Fig. 2a, right**, excludes mosaic embryos, p=0.015). It is widely accepted that CRISPR/Cas9-
98 mediated editing efficiency can be locus- and guide-dependent, so we tested the effects of
99 RAD51 on KI efficiencies at a second genomic locus to confirm its effects. Using the same
100 strategy employed for *Chd2*, we attempted to knock in an albinism-associated human mutation
101 (c.265T>A; C89S; hereon referred to as Tyr^{C89S}; schematic in **Fig. 2b**) in the *Tyr* gene[13], which
102 encodes for tyrosinase, the rate-limiting enzyme in melanin production. Albinism is a recessive
103 disorder and, as such, only homozygous disruption of *Tyr* results in mice completely lacking
104 pigment (**Fig. 2c**). Because homozygous indels in *Tyr* can also result in albinism, all F_0 animals
105 were genotyped to assess the effects of RAD51 on KI efficiencies (**Fig. 2d**) and phenotyped
106 (**Extended Data Table 2)** to assess mosaicism. In the case of mosaic animals, genotyping was
107 performed using tissue completely lacking melanin to assess the number of animals with a
108 homozygous KI event (**Fig. 2e, middle)**. Injections without RAD51 showed a high overall KI
109 efficiency and this efficiency was not significantly increased by the addition of RAD51 (**Fig. 2e,**
110 **left**). However, our genotyping results showed that RAD51 enhances homozygous KI efficiency,
111 with 44% of pups (including mosaics) having an albino phenotype resulting specifically from
112 homozygous KI of the Tyr^{C89S} allele with RAD51, as compared to only 12% without (**Fig. 2e,**
113 **middle**, one-tailed chi-square test, p=0.0081). Furthermore, RAD51 co-injection increased the
114 number of pure homozygous KI animals (**Fig. 2e, right,** one-tailed chi-square test, p=0.027),
115 supporting our findings at the *Chd2* locus indicating that RAD51 can enhance homozygous KI.

116 Strikingly, RAD51 co-injection more than doubled the observed homozygosity at both
117 the *Chd2* and *Tyr* loci, regardless of whether or not we took mosaicism into account (**Fig. 2a,e**).
118 Previous attempts to increase HDR through pharmacological or genetic mechanisms have not
119 shown such high homozygosity rates[3,7,14], leading us to investigate the mechanism by which
120 RAD51 can promote such an outcome. Our evidence that RAD51 only marginally increases the
121 overall efficiency of ssODN-mediated knock-in (**Fig. 2a,e**) following PNI suggested that its
122 effects on homozygosity do not come from increasing independent KI events on both alleles.
123 Additionally, due to the random nature of indels produced by non-homologous end joining
124 (NHEJ), we found it surprising that we observed multiple embryos from both $Chd2^{R1684H}$ and
125 Tyr^{C89S} injections whose genotyping results suggested the presence of the same indel on both
126 alleles (**Extended Data Table 1,2**). Genotyping of F_1 pups derived from a *Chd2*-targeted female
127 with such a homozygous indel revealed that all pups were heterozygous for the same indel,
128 confirming that the homozygosity of the founder (**Extended Data Fig. 2**). Although we could
129 not completely rule out that these deletions were generated by MMEJ, which can result in
130 stereotyped indels based on local homology[2,15], the variety of observed indels and a lack of
131 MMEJ sequence motifs at the R1684H editing site suggest that the homozygosity resulted from
132 recombination between homologs that transferred the indel from one chromosome to the other.
133 More than 20 years ago, experiments in mouse ES cells found evidence of recombination
134 events between homologous chromosomes[16,17]. While these interhomolog repair (IHR) events
135 are well-understood in meiotic cells, their occurrence in zygotes and somatic cells is poorly
136 described. Furthermore, experiments investigating IHR in somatic cells have shown that it occurs
137 at very low frequencies[11,12]. However, several recent studies have described zygotic IHR events
138 after induction of a targeted double-strand breaks (DSBs) by Cas9[18,19]. Based on these data, we

139 hypothesized that RAD51 promotes homozygous KI through a similar mechanism. To directly
140 test this, we attempted to generate homozygous *Chd2*^{R1684H} embryos through editing of
141 *Chd2*$^{R1684/+}$ embryos without the use of an exogenous donor. Using wildtype C57BL/6N eggs
142 and sperm from homozygous *Chd2*^{R1684H} male mice, we generated heterozygous zygotes via IVF
143 and specifically targeted Cas9 to the wildtype maternal *Chd2* locus. As illustrated in **Figure 3a**,
144 paternal PNI was performed on zygotes ~8 hours post fertilization (hpf) using a mixture of
145 crRNA, tracrRNA, and Cas9 with or without RAD51. The *Chd2*^{R1684H} allele contains mutations
146 in both the guide sequence and its associated PAM and we confirmed through *in vitro* digestion
147 assays that Cas9 is only capable of cutting the wildtype maternal allele (**Extended Data Fig. 3**).
148 By omitting a donor template from the injection mixture, we were able to directly test both the
149 rate of baseline CRISPR/Cas9-mediated IHR in zygotes and the ability of RAD51 to enhance
150 such a mechanism. In agreement with previous work demonstrating IHR in human zygotes[18],
151 including mosaic embryos we observed IHR events in 26% of control-injected embryos (**Fig.
152 3b,c**). Strikingly, co-injection of RAD51 increased this rate to 74% (**Fig. 3c, left**, one-tailed chi-
153 square test, $p<0.0001$). Analysis of the rates of embryos with pure, non-mosaic IHR events
154 showed a similar increase in IHR rates in RAD51-injected embryos (**Fig. 3c, right**, one-tailed
155 chi-square test, $p=0.009$), supporting the hypothesis that RAD51 can promote IHR in mouse
156 zygotes.

157 Previous studies analyzing the properties of indels observed in single sgRNA-based
158 CRISPR experiments have shown that indels large enough to disrupt our genotyping strategy are
159 too infrequent to account for the loss-of-heterozygosity observed in our experiments[20].
160 Nonetheless, we performed multiple experiments to directly rule out the possibility of false
161 positives resulting from monoallelic deletions on the maternal allele[21]. First, we developed and

162 performed a multiplex genomic qPCR assay to analyze copy number at the targeted locus (**see**
163 **Methods**). Using genomic DNA from wildtype mice and *Shank3B*$^{+/-}$ mice harboring a
164 heterozygous deletion of exon 13 of *Shank3*[22], we confirmed that our method was capable of
165 identifying heterozygous deletions **(Fig. 3d)**. We then confirmed that PCR targeting the
166 *Chd2*^{R1684H} locus is sensitive enough to detect relevant changes in copy-number by halving the
167 input DNA used for the assay (**Fig. 3d**). Finally, using this genomic qPCR strategy we were able
168 to confirm normal copy-number at the R1684H locus in 5/5 randomly selected pure homozygous
169 mutants (**Fig. 3d**). Next, we generated F_0 *Chd2*$^{R1684H/R1684H}$ animals via the IVF strategy
170 described in **Figure 3a** (including RAD51) and crossed homozygotes with wildtype C57BL/6N
171 mice to generate F_1 animals. Genotyping of F_1 offspring confirmed that 100% were heterozygous
172 for the R1684H mutation (**Fig. 3e**), supporting the conclusion that the F_0 animals were
173 homozygotes generated via IHR. Although we cannot rule out the possibility that a small fraction
174 of embryos contain large hemizygous deletions, our results strongly support the conclusion that
175 RAD51 is capable of stimulating highly-efficient zygotic IHR.

176 After fertilization, the maternal and paternal pronuclei remain physically separated until
177 the completion of S-phase, at which time they fuse in preparation for mitosis. This poses a
178 significant problem given that an IHR mechanism requires physical association of the maternal
179 and paternal chromosomes and suggests that IHR must occur after S-phase. Because genotyping
180 analyses of one-cell stage embryos are difficult to interpret due to failed PCR amplification of
181 alleles harboring a Cas9-induced DSB, we chose to test the timing of zygotic IHR via
182 immunocytochemistry (ICC) for RAD51 in uninjected, RAD51-injected, Cas9-injected (with
183 *Chd2*-targeting crRNA), and Cas9- and RAD51-injected zygotes at three stages of the cell cycle:
184 G1, , G2 (post S-phase), and M-phase (see **Methods**). Previous studies have shown that RAD51

185 staining is weak and/or diffuse in wildtype cells, but that strong RAD51 puncta appear in
186 response to DSBs[23]. In agreement with our genotyping data and the hypothesis that IHR occurs
187 after S-phase, we observed the appearance of RAD51 puncta solely during G2 (**Fig. 4a,b**).
188 Although we did not observe RAD51 puncta in any uninjected G2 embryos, we were surprised to
189 see several embryos injected solely with RAD51 that exhibited strong RAD51 foci (**Fig. 4b**).
190 The appearance of such foci only after S-phase suggests that increasing levels of RAD51 can
191 bias the cell toward RAD51-mediated repair over endogenous RAD52-dependent mechanisms
192 for repairing replication-associated DSBs in mammals[24]. However, embryos injected with Cas9
193 showed a significantly increased frequency of RAD51 puncta and the highest proportion of
194 positively-stained embryos was observed in the group injected with both Cas9 and RAD51 (**Fig.
195 4b, Extended Data Table 3**). Furthermore, embryos injected with RAD51 alone only exhibited
196 single RAD51 puncta, but Cas-injected embryos were often observed with 2 or more puncta
197 (**Extended Data Fig. 4**), indicative of IHR events on both maternal alleles, as well as at potential
198 off-target Cas9-induced DSBs. While these findings suggest a model whereby RAD51 stimulates
199 IHR in zygotes during G2, a deeper understanding of the pathways involved in IHR is still
200 necessary.

201 To gain a deeper understanding of the pathways involved in zygotic IHR, we performed a
202 series of injections in Cas9-injected *Chd2*$^{R1684H/+}$ zygotes with multiple DSB repair- and
203 homologous recombination (HR)-associated proteins: USP1/WDR48 (promotes HR via
204 Fanconi-Anemia (FA) pathway[25]), BCCIP (promotes BRCA2-mediated HR[26-28], participates in
205 FA pathway[29]), XRCC1 (promotes MMEJ and co-localizes with RAD51[30,31]), XRCC4 (promotes
206 NHEJ and regulator of V(D)J recombination[32,33]), and DMC1 (meiotic HR regulator[34]). XRCC1,
207 XRCC4, and DMC1 were not capable of inducing IHR at rates above baseline (**Fig. 4c**),

208 confirming the specificity of RAD51 and indicating that zygotic IHR pathways do not utilize
209 proteins typically related to HR-independent DSB repair. Co-injection of USP1/WDR48, on the
210 other hand, was capable of significant enhancement of IHR (**Fig. 4c**). Strikingly, BCCIP
211 exhibited a significantly stronger effect on IHR rates than USP1/WDR48 (one-tailed chi-square
212 test, p=0.0014), with 95% of edited embryos showing IHR (**Fig. 4c**). Since BCCIP-mediated
213 activation of BRCA2 promotes RAD51 activation, these data suggest that proteins capable of
214 directly affecting RAD51 activity are likely to promote high-efficiency IHR. Additionally, the
215 ability of the FA pathway members BCCIP, USP1/WDR48, and RAD51 to enhance zygotic IHR
216 implicates the FA pathway in this process.

217 *RAD51* mutations have been identified in multiple human cancers and Fanconi-Anemia
218 and several of these mutations have been studied in-depth. In an effort to better understand the
219 role of RAD51 in IHR, we co-injected three different recombinant RAD51 mutant proteins with
220 Cas9 and *Chd2*^{R1684H} crRNA into IVF-generated *Chd2*$^{R1684H/+}$ embryos. The mutants were as
221 follows: T131P (deficient in interstrand crosslink repair (ICL), but not HR[35,36]), SA208-209ED
222 (disrupted BRCA2-association[37]), and G151D (gain-of-function mutant with increased strand
223 exchange activity[38]). T131P injection was not capable of increasing IHR frequency compared to
224 Cas9-only embryos (**Fig. 4d**), indicating that RAD51 function associated with ICL repair is
225 required for the induction of IHR. Likewise, SA208-209ED showed unchanged IHR rates
226 compared to Cas9-only embryos (**Fig. 4d**), supporting a role for BRCA2 in RAD51-mediated
227 promotion of IHR. Surprisingly, in 27 zygotes injected with the RAD51 gain-of-function variant,
228 we did not record a single indel event and observed IHR in all edited cells (**Fig. 4d**). However,
229 the apparent editing efficiency dropped to 22% (**Fig. 4e**), suggesting that G151D either directly
230 inhibits Cas9 nuclease activity or stimulates IHR at such high levels that the replicated wildtype

231 maternal allele is often used as a template. To test whether G151D can directly inhibit Cas9
232 activity, we performed *in vitro* Cas9 digestion assays with and without co-incubation with
233 G151D and did not observe any direct inhibition of Cas9 activity (**Fig. 4f**). Interestingly, we
234 observed a similar decrease in editing efficiency with BCCIP-injected embryos that was not due
235 to direct inhibition of Cas9 activity (**Fig. 4f, Extended Data Fig. 5**). Additional analyses of
236 overall indel rates and the indel-to-IHR ratios in embryos injected with RAD51, BCCIP, or
237 RAD51 G151D revealed a drastic decrease in both rates compared to control embryos (**Fig.
238 4g,h**). Furthermore, both BCCIP and RAD51 G151D embryos showed significant decreases in
239 these rates compared to embryos injected with wildtype RAD51. Our previous experiments
240 demonstrated that IHR occurs after S-phase in zygotes, when a second wildtype allele is present
241 to serve as an IHR template. Therefore, our data argue that rather than inhibiting Cas9-mediated
242 DSBs, BCCIP and the RAD51 G151D mutant stimulate IHR with nearly 100% efficiency and
243 indel-to-IHR ratios near zero.

244 Our data demonstrate that RAD51, the BRCA2-interacting protein BCCIP, and the FA
245 pathway-associated protein complex of USP1 and WDR48 are capable of significantly
246 enhancing the rate of zygotic interhomolog repair. Our mechanistic characterization of IHR in
247 zygotes suggests a model whereby Cas9-induced DSBs are repaired through the use of a
248 homologous chromosome as a template during G2. At this time, the maternal and paternal
249 genomes have already undergone replication and the pronuclei undergo fusion prior to the start
250 of M-phase. This creates a significant hurdle for pure, non-mosaic IHR, as the cell must now edit
251 two alleles instead of one. This is highlighted by the high degree of mosaicism observed in
252 embryos exhibiting IHR (**Extended Data Fig. 6**). Interestingly, although BCCIP-injected
253 embryos exhibited a significant increase in mosaicism, only 1 out of 14 BCCIP-injected embryos

254 with mosaic IHR was mosaic with an indel (**Extended Data Fig. 6c,d**), suggesting that BCCIP
255 protects against indels by greatly increasing the likelihood of repairing DSBs through IHR
256 instead of NHEJ. Together, our mosaicism analyses support our ICC results showing that zygotic
257 IHR occurs following pronuclear fusion when there are multiple IHR templates available for
258 repair.

259 Single-cell RNA-sequencing has shown that *Rad51* mRNA is present in zygotes at
260 relatively low levels (FPKM <50)[39]. Nonetheless, the existence of endogenous RAD51 in
261 zygotes begs the question of exactly how exogenous RAD51 enhances IHR. We hypothesize
262 based on the data presented in this paper that increased concentrations of RAD51 in zygotic
263 pronuclei increase the probability of RAD51 locating and binding to a DSB. While previous
264 work has shown that accumulation of endogenous RAD51 at zygotic DSBs can occur in genetic
265 models of genomic instability, we did not observe any RAD51 puncta in uninjected cells at any
266 stage of the cell cycle. However, injection of RAD51 protein alone revealed a small number of
267 cells with RAD51 puncta (**Fig. 4b**), suggesting that increasing RAD51 levels is capable of
268 biasing repair of endogenous DSBs toward RAD51-dependent pathways. The highly-efficient,
269 indel-free editing observed in cells injected with the G151D mutant further supports this
270 mechanism where increased concentrations of RAD51 promote IHR by increasing the likelihood
271 of RAD51 binding to a DSB. Although we injected the same concentration of G151D into cells
272 as we did wildtype RAD51, the G151D mutant has a faster on-rate for binding DSBs and binds
273 DSBs more stably due to its increased strand-exchange activity[38] and decreased rate of ATP
274 hydrolysis[40], respectively. This could help explain why we do not observe indels in these cells, as
275 G151D is likely capable of binding Cas9-induced DSBs faster and for longer periods of time
276 than other DNA repair molecules after the completion of S-phase.

277 Our insights into the basic mechanisms of IHR in zygotes suggest that enhanced IHR has
278 the potential to overcome current problems limiting the feasibility of gene drive strategies. Gene
279 drives are designed to edit wild populations for disease prevention and agricultural purposes by
280 accelerating the spread of alleles conferring desired traits. They consist of a single locus
281 encoding a gene of interest, Cas9, and an sgRNA targeting the same wildtype locus. In
282 heterozygotes, expression of Cas9 and the sgRNA targets Cas9 to the wildtype allele, inducing a
283 DSB that can be repaired through IHR to generate cells homozygous for the gene drive cassette.
284 This conversion of heterozygotes to homozygotes is key to the success of gene drives, but recent
285 work has demonstrated the rapid development of gene drive resistance through the production of
286 undesired indels that prevent cutting and subsequent IHR[41,42]. Therefore, our discovery that
287 BCCIP and RAD51 G151D promote nearly indel-free IHR in zygotes has enormous potential for
288 overcoming the barriers to successful gene drive applications. Furthermore, the same advantages
289 of indel-free IHR could be used to develop safe gene therapies for autosomal dominant disorders
290 caused by point mutations and small indels. Given that we still know so little about endogenous
291 mechanisms of IHR, the potential impact of our findings suggests that additional studies of IHR
292 in zygotes and somatic cells will be fundamental to the development of improved tools and
293 strategies for gene editing.
294

295 **Methods**

296 ***Data Availability:*** The raw data supporting the findings in this manuscript can be obtained from
297 the corresponding author upon reasonable request.

298 ***Animal Care and Use:*** All mouse work was performed with the supervision of the
299 Massachusetts Institute for Technology Division of Comparative Medicine (DCM) under

300 protocol 0416-024-19, which was approved by the Committee for Animal Care (CAC). All
301 procedures were in accordance with the guidelines set forth by the Guide for Care and Use of
302 Laboratory Animals, National Research Council, 1996 (institutional animal assurance no. A-
303 3125-01). All embryos injected for the experiments described in this manuscript were on a
304 C57BL/6NTac background (Taconic; referred to as C57BL/6N in paper).
305 ***Preparation of Injection Mixtures***: tracrRNA, crRNAs, and ssODNs were synthesized by
306 Integrated DNA Technologies (see **Supplementary Table 1** for sequences). All injection
307 mixtures were prepared in a final volume of 50µL according using the same protocol. Using
308 RNase-free water, reagents, and consumables, crRNA (final concentration 0.61µM), tracrRNA
309 (final concentration 0.61µM), and ultrapure Tris-HCl, pH7.39 (final concentration 10mM,
310 ThermoFisher) were mixed and incubated at 95°C for 5 minutes. The mixtures were cooled to
311 room temperature for 10 minutes on the benchtop and then EnGen Cas9 NLS, *S. pyogenes* (New
312 England Biolabs) was added to a final concentration of 30ng/µL. The mixtures were incubated at
313 37°C for 15 minutes before adding any remaining components: ssODN (final concentration
314 30ng/µL), RAD51 (Creative Biomart, final concentration 10ng/µL). Injection mixtures were
315 stored on ice and briefly heated to 37°C prior to injection. For experiments utilizing RS-1,
316 embryos were cultured in KSOM-AA (EMD Millipore MR-121-D) with 7.5µM RS-1 (Sigma)
317 dissolved in DMSO or DMSO (Sigma, 1:1000) for 24 hours, washed, and cultured in
318 EmbryoMax FHM HEPES Buffered Medium (Sigma) until collection for genotyping.
319 ***Recombinant Proteins:*** For experiments using wildtype recombinant proteins, the following
320 proteins were used: RAD51 (Creative Biomart RAD51-134H), USP1/WDR48 (Creative
321 Biomart USP1&WDR48-1067H), BCCIP (Origene TP303061), XRCC1 (TP304952), XRCC4
322 (Origene TP312684), DMC1 (Origene TP318311). For experiments using mutant RAD51,

323 custom RAD51 preparations were produced by Creative Biomart according to their standard
324 protocol for producing the wildtype RAD51 used in all other experiments. DNA sequences used
325 for cloning the mutant forms of *Rad51* are described in **Supplementary Table 2**. All RAD51
326 mutants were modeled in human *RAD51* transcript variant 4 (NCBI accession NM_001164269),
327 as this is the transcript variant of the wildtype RAD51-134H protein used in all other
328 experiments.
329 ***Natural Mating for Zygotic Injections:*** Female mice (4-5 weeks old, C57BL/6N) were
330 superovulated by IP injection of PMS (5 IU/mouse, three days prior to microinjection) and hCG
331 (5 IU/mouse, 47 hours after PMS injection) and then paired with males. Plugged females were
332 sacrificed by cervical dislocation at day 0.5pcd and zygotes were collected into 0.1%
333 hyaluronidase/FHM (Sigma). Zygotes were washed in drops of FHM and cumulus cells were
334 removed. Zygotes were cultured in KSOM-AA for one hour and then used for microinjection.
335 ***In Vitro Fertilization for Zygotic Injections***: *In vitro* fertilization was performed using
336 FERTIUP® Mouse Preincubation Medium and CARD MEDIA (Kyudo Company) according to
337 the manufacturer's protocol. Non-virgin *Chd2*$^{R1684H/R1684H}$ males that were >8 weeks old were
338 used as sperm donors. Following IVF, embryos were cultured for 8 hours and then injected using
339 the PNI protocol described below.
340 ***Zygotic Microinjections***: For all experiments except the CPI experiments described in **Fig. 1**,
341 the male pronucleus was injected. Injections performed for the CPI portion of **Fig. 1** were
342 targeted to the cytoplasm. All microinjections were performed using a Narishige
343 Micromanipulator, Nikon Eclipse TE2000-S microscope, and Eppendorf 5242 microinjector.
344 Individual zygotes were injected with 1-2pL of injection mixture using an "automatic" injection
345 mode set according to needle size and adjusted for clear increase in pronuclear volume.

346 Following injections, cells were cultured in KSOM-AA until collection for genotyping. For
347 experiments giving rise to F_0 animals, embryos were surgically implanted into pseudopregnant
348 CD-1 females (Charles River Laboratories, Strain Code 022) 24-hours post-injection and allowed
349 to develop normally until natural birth.

350 ***Embryo Collection and DNA Purification***: Embryos were collected at morula-to-blastocyst
351 stage in 4µL nuclease-free water. After collection, 4µL of 2X embryo digestion buffer was added
352 to each sample (final concentrations: 125µg/mL proteinase K, 100mM Tris-HCl pH 8.0, 100mM
353 KCl, 0.02% gelatin, 0.45% Tween-20, 60µg/mL yeast tRNA) and embryos were lysed for 1 hour
354 at 56°C. Proteinase K was inactivated via incubation at 95°C for 10 minutes and DNA was
355 stored at -20°C until use.

356 ***Tail DNA Purification***: Tail tissue (~0.5cm length) was collected from individual animals,
357 placed in 75µL alkaline lysis buffer (25mM NaOH, 0.2mM EDTA), and incubated at 95°C for
358 30 minutes. Digestion was stopped via addition of 75µL neutralization buffer (40mM Tris-HCl
359 pH 5.0). Samples were stored at 4°C until genotyping.

360 ***Chd2^{R1684H} PCR*:** *Chd2^{R1684H}* genotyping was performed via a two-step, nested approach. Except
361 for experiments described in **Figure 3**, all 8µL of embryo DNA were used as input for the initial,
362 long round of PCR. Genotyping of mouse pups and adult animals was performed using 2µL of
363 purified tail DNA. For all embryo genotyping, reactions mixtures were set up in a UV-sterilized
364 laminar flow hood using sterile reagents and filter tips to avoid contamination. All PCR was
365 performed using Biolase DNA Polymerase (Bioline), fresh aliquots of dNTPs (New England
366 Biolabs), and 2% DMSO (final concentration). The first PCR reaction of the nested PCR was
367 performed using the C2RH-Long_F/R primer pairs listed in **Supplementary Table 3**. Primer
368 pairs C2RH-Long_F1/R1 and C2RH-short_F1/R1 were used for **Figures 1-3**, as well as

369 **Extended Data Figures 1 and 2**. All other experiments utilized primer pairs C2RH-
370 Long_F2/R2 and C2RH-short_F2/R2, which was designed to amplify a larger genomic region as
371 a way to further rule out large deletions that could disrupt PCR primer binding sites. 20 cycles of
372 amplification were performed using 30 second extension and annealing times and an annealing
373 temperature of 67°C. Nested PCR was then performed using 2µL of the initial 25µL PCR
374 reaction as input. The C2RH-Short_F/R primer pairs listed in **Supplementary Table 3** were
375 used for this PCR, with sets 1 and 2 being used as described above. Thirty-five cycles of
376 amplification were performed using 30 second extension and annealing times and an annealing
377 temperature of 68°C.
378 ***Tyr^{C89S} PCR:*** Initial PCR was performed using 2µL purified tail DNA. The longer amplification
379 of the nested PCR reaction was performed using the Tyr-Long_F/R primer pair listed in
380 **Supplementary Table 3**. PCR was performed using Biolase DNA polymerase (Bioline) and a
381 final concentration of 2% DMSO. Twenty cycles of PCR were run with 30 second annealing and
382 extension steps and an annealing temperature of 66°C. Nested PCR was performed using 2µL of
383 the initial 25µL PCR reaction and the Tyr-Short_F/R primer pair listed in **Supplementary Table**
384 **3**. The same PCR conditions were used for the nested PCR as were used for the initial PCR.
385 ***Sanger Sequencing:*** For all sequencing reactions, 5µL of PCR product was mixed with 3µL
386 dH_2O and 2µL ExoSAP (Exonuclease I, NEB #M0293 and rSAP, NEB #M0371). Products were
387 incubated at 37°C for 30 minutes to degrade primers and dephosphorylate dNTPs and enzymes
388 were then heat inactivated at 80°C for 15 minutes. 2.5µL dH_2O and 2.5µL 10µM sequencing
389 primer were then added to each mixture and samples were submitted to Genewiz for Sanger
390 sequencing. Sequence files (.ab1) were blinded using a freely-available Perl script
391 (https://github.com/jimsalterjrs/blindanalysis) and analyzed using SnapGene. To identify IHR

392 events in mosaic samples, we monitored the genotype at the R1684H locus, as well as the PAM
393 site and compared the major and minor peak heights using 4Peaks (Nucleobytes). Sequences
394 showing >2:1 ratio of major allele to minor allele at both sites were called IHR-positive, but
395 mosaic. Sequencing primers used were: Chd2-Short_R1, Chd2-Short_F2, and Tyr-Short_F (see
396 **Supplementary Table 3**).
397 ***Total Protein Staining and Western Blotting:*** 1μg of each recombinant protein was mixed with
398 2X Laemmli Sample Buffer (Bio-Rad) and heated to 95°C for 5 minutes. After brief
399 centrifugation, samples were loaded into 4-15% Mini-PROTEAN TGX Pre-Cast gels (Bio-Rad)
400 along with 5μL PrecisionPlus Protein Kaleidoscope Prestained Protein Standards (Bio-Rad) and
401 run at 200V for 40 minutes in 1X Tris/Glycine/SDS running buffer. Protein was transferred to
402 nitrocellulose at 100V for 1 hour at 4°C and total protein was visualized using REVERT Total
403 Protein Stain (LI-COR Biosciences) according to the manufacturer's protocol. For RAD51
404 Western blotting in **Supplementary Figure 1a**, REVERT Total Protein Stain was reversed
405 according to the manufacturer's protocol, the membrane was blocked at room temperature for 1
406 hour in TBST containing 5% non-fat dry milk. Primary antibody (Rb anti-RAD51, Abcam
407 ab63801, 1:500) was diluted in blocking buffer and applied to the membrane overnight at 4°C.
408 Following washes with TBST, secondary antibody (IRDye 800CW Gt anti-rabbit IgG H+L, LI-
409 COR 925-32211, 1:15,000) was diluted in blocking buffer and applied to the membrane for 1
410 hour at room temperature in the dark. The membrane was then washed and imaged. For all
411 experiments, imaging was performed on an Odyssey CLx Imaging System with ImageStudio
412 (LI-COR Biosciences). Coomassie staining and Western blots in **Supplementary Figure 1b**
413 were performed by Creative Biomart.

414 ***In vitro Cas9 Digestion Assays:*** Wildtype or *Chd2*$^{R1684H/R1684H}$ genomic DNA was used as input
415 for PCR using the conditions described above and the primers specified in **Supplementary**
416 **Table 3**. After confirmation of a single band via gel electrophoresis, the PCR reactions were
417 purified using the DNA Clean & Concentrator kit (Zymo) according to the manufacturer's
418 instructions. crRNA and tracrRNA were diluted 1µM in Nuclease-free Duplex Buffer (IDT) and
419 incubated at 95°C for 5 minutes before being allowed to cool to room temperature on the bench.
420 Digestion mixtures were made in separate tubes by combining nuclease-free water, 10X Cas9
421 Nuclease Reaction Buffer (final concentration 1X, New England Biolabs), 1µL of the cooled
422 crRNA/tracrRNA duplex, and, if necessary, 1µL of EnGen Cas9 NLS, *S. pyogenes* (New
423 England Biolabs). These mixtures were heated to 37°C for 10 minutes before adding 250ng PCR
424 product and, if necessary, RAD51 G151D (10ng/µL final concentration, custom-produced by
425 Creative Biomart) or BCCIP (10ng/µL final concentration, Origene TP303061). Digestion was
426 performed at 37°C for 1 hour, Cas9 was denatured at 95°C, 6X Purple Gel Loading Dye (New
427 England Biolabs) was added to a final concentration of 1X, and the samples were allowed to
428 passively cool to room temperature. After cooling, reactions were separated via electrophoresis
429 with 2% agarose gel, post-stained with GelRed Nucleic Acid Gel Stain (Biotium) according to
430 manufacturer's instructions and visualized using an InGenius Gel Documentation System
431 (Syngene).
432 ***Genomic qPCR****:* To determine copy number at specific genomic loci, we developed a strategy
433 utilizing multiplex nested qPCR. We first performed multiplex amplification of both the edited
434 *Chd2* region and a region of the *Gapdh* promoter, which is located on a different chromosome, in
435 a short round of PCR (10 cycles). In the case of our *Shank3B* control experiment, we attempted
436 to match the input DNA concentration used for experiments utilizing DNA from cultured

437 embryos. Based on an estimation of ~6pg DNA per cell and a PCR input of ~30 cells, we used
438 180pg *Shank3B*$^{+/+}$ or *Shank3B*$^{+/-}$ genomic DNA per initial reaction using the Shank3-Long-F/R
439 and Gapdh-Long_F/R primer pairs described in **Supplementary Table 3**. We then used the PCR
440 products from the initial multiplex PCR as input for nested qPCR using the Shank3-Short_F/R
441 and Gapdh-Short_F/R primer pairs with Sso Advanced SYBR Green Supermix (Bio-Rad). qPCR
442 was performed on a CFX96 Touch Real-Time PCR Detection System (Bio-Rad) and analyzed
443 using CFX Maestro software (Bio-Rad). *Shank3B* signal was normalized to *Gapdh* signal to
444 control for input and a second diploid locus. In a second control experiment to test qPCR
445 sensitivity at the *Chd2* locus, we isolated DNA from wildtype blastocysts and performed
446 multiplex PCR for *Chd2* using the C2RH-Long_F1/R1 and Gapdh-Long_F/R primer pairs listed
447 in **Supplementary Table 3**. We then performed genomic qPCR using the same input amount for
448 *Gapdh* nested qPCR (Gapdh-Short_F/R primers), but either 1X or 0.5X input for the *Chd2*
449 nested qPCR (Chd2-Short_F1/R1 primers). Finally, we used the same strategy to perform nested
450 genomic qPCR using genomic DNA isolated from 5 randomly-selected blastocysts that had
451 genotyped positive for interhomolog repair with no evidence of mosaicism.
452 ***Immunocytochemistry:*** Zygotes were collected during G1 (9hpf, 1hpi, PN2), G2 (14.5hpf,
453 6.5hpi, PN5), or M-phase (16hpf, 8hpi) and fixed overnight at 4°C in 4% PFA + 0.1% Tween-20
454 in PBS and then briefly transferred to acidified Tyrode's (Sigma T1788) to remove the zona.
455 Collection times and cell cycle stages were determined empirically based on pronuclear/nuclear
456 morphology[43]. After washing in PBS + 0.1% Tween-20 (PBST), zygotes were permeabilized in
457 PBS + 1% Triton X-100 for 1 hour at 4°C and then blocked for 1 hour at room temperature in
458 blocking solution (PBS + 3% BSA + 5% normal goat serum). Primary antibody (rabbit anti-
459 RAD51, Abcam ab63801, 1:500) was diluted in blocking solution and applied to coverslips

460 overnight at 4°C. Cells were washed 3 times in PBST before application of secondary antibody
461 (goat anti-rabbit IgG conjugate, Alexa Fluor 488, ThermoFisher A-11008) diluted in blocking
462 solution for 1 hour at room temperature. Nuclei were counterstained with DAPI and coverslips
463 were mounted to slides with Fluoromount Aqueous Mounting Medium (Sigma F4680). Cells
464 were imaged on an Olympus Fluoview FV1000 confocal microscope with a 60X oil immersion
465 objective and variable digital zoom. For all cells, we acquired z-stacks incorporating both
466 pronuclei. Raw image files were exported to FIJI[44] for Z-projection (sum slices), channel
467 splitting, and scale bar generation.

468 ***Statistical Analyses***: Statistical analyses were performed using Prism 6 (Graphpad). For chi-
469 square analyses, one-tailed tests were used in cases where we were testing whether a factor could
470 specifically increase interhomolog repair. For all other experiments, two-tailed analyses were
471 performed. Details on statistical tests performed for each experiment are provided in text and
472 figure legends. All graphs display mean±SEM. *$p<0.05$, **$p<0.01$, ***$p<0.001$, ****$p<0.0001$

473

474 **References**

475

476 1. Aida, T. *et al.* Cloning-free CRISPR/Cas system facilitates functional cassette
477 knock-in in mice. *Genome Biol* **16,** 87 (2015).
478 2. Aida, T. *et al.* Gene cassette knock-in in mammalian cells and zygotes by enhanced
479 MMEJ. *BMC Genomics* **17,** 183 (2016).
480 3. Paquet, D. *et al.* Efficient introduction of specific homozygous and heterozygous
481 mutations using CRISPR/Cas9. *Nature* **533,** 125–129 (2016).
482 4. Li, G. *et al.* Small molecules enhance CRISPR/Cas9-mediated homology-directed
483 genome editing in primary cells. *Sci. Rep.* **7,** 8943 (2017).
484 5. Yu, C. *et al.* Small Molecules Enhance CRISPR Genome Editing in Pluripotent
485 Stem Cells. *Cell Stem Cell* **16,** 142–147 (2015).
486 6. Song, J. *et al.* RS-1 enhances CRISPR/Cas9- and TALEN-mediated knock-in
487 efficiency. *Nature Communications* **7,** 10548 (2016).
488 7. Maruyama, T. *et al.* Increasing the efficiency of precise genome editing with
489 CRISPR-Cas9 by inhibition of nonhomologous end joining. *Nature Biotechnology*
490 **33,** 538–542 (2015).

491 8. Ma, X. *et al.* CRISPR/Cas9-mediated gene manipulation to create single-amino-
492 acid-substituted and floxed mice with a cloning-free method. *Sci. Rep.* **7,** 42244
493 (2017).
494 9. Quadros, R. M. *et al.* Easi-CRISPR: a robust method for one-step generation of mice
495 carrying conditional and insertion alleles using long ssDNA donors and CRISPR
496 ribonucleoproteins. *Genome Biol* **18,** 103 (2017).
497 10. Schwacha, A. & Kleckner, N. Interhomolog bias during meiotic recombination:
498 meiotic functions promote a highly differentiated interhomolog-only pathway. *Cell*
499 **90,** 1123–1135 (1997).
500 11. Stark, J. M. & Jasin, M. Extensive loss of heterozygosity is suppressed during
501 homologous repair of chromosomal breaks. *Mol Cell Biol* **23,** 733–743 (2003).
502 12. LaRocque, J. R. *et al.* Interhomolog recombination and loss of heterozygosity in
503 wild-type and Bloom syndrome helicase (BLM)-deficient mammalian cells.
504 *Proceedings of the National Academy of Sciences* **108,** 11971–11976 (2011).
505 13. Ghodsinejad Kalahroudi, V. *et al.* Two Novel Tyrosinase (TYR) Gene Mutations
506 with Pathogenic Impact on Oculocutaneous Albinism Type 1 (OCA1). *PLoS ONE* **9,**
507 e106656 (2014).
508 14. Takayama, K. *et al.* Highly efficient biallelic genome editing of human ES/iPS cells
509 using a CRISPR/Cas9 or TALEN system. *Nucleic Acids Research* **45,** 5198–5207
510 (2017).
511 15. McVey, M. & Lee, S. E. MMEJ repair of double-strand breaks (director's cut):
512 deleted sequences and alternative endings. *Trends in Genetics* **24,** 529–538 (2008).
513 16. Richardson, C., Moynahan, M. E. & Jasin, M. Double-strand break repair by
514 interchromosomal recombination: suppression of chromosomal translocations.
515 *Genes & Development* **12,** 3831–3842 (1998).
516 17. Moynahan, M. E. & Jasin, M. Loss of heterozygosity induced by a chromosomal
517 double-strand break. *Proc Natl Acad Sci USA* **94,** 8988–8993 (1997).
518 18. Ma, H. *et al.* Correction of a pathogenic gene mutation in human embryos. *Nature*
519 **548,** 413–419 (2017).
520 19. Wu, Y. *et al.* Correction of a Genetic Disease in Mouse via Use of CRISPR-Cas9.
521 *Cell Stem Cell* **13,** 659–662 (2013).
522 20. Shin, H. Y. *et al.* CRISPR/Cas9 targeting events cause complex deletions and
523 insertions at 17 sites in the mouse genome. *Nature Communications* **8,** 15464
524 (2017).
525 21. Egli, D. *et al.* Inter-homologue repair in fertilized human eggs? *biorxiv.org*
526 doi:10.1101/181255
527 22. Peca, J. *et al.* Shank3 mutant mice display autistic-like behaviours and striatal
528 dysfunction. *Nature* **472,** 437–442 (2011).
529 23. Ladstätter, S. & Tachibana-Konwalski, K. A Surveillance Mechanism Ensures
530 Repair of DNA Lesions during Zygotic Reprogramming. *Cell* **167,** 1774–1787.e13
531 (2016).
532 24. Sotiriou, S. K. *et al.* Mammalian RAD52 Functions in Break-Induced Replication
533 Repair of Collapsed DNA Replication Forks. *Mol. Cell* **64,** 1127–1134 (2016).
534 25. Murai, J. *et al.* The USP1/UAF1 complex promotes double-strand break repair
535 through homologous recombination. *Mol Cell Biol* **31,** 2462–2469 (2011).

536 26. Lu, H. *et al.* The BRCA2-Interacting Protein BCCIP Functions in RAD51 and
537 BRCA2 Focus Formation and Homologous Recombinational Repair. *Mol Cell Biol*
538 **25,** 1949–1957 (2005).
539 27. Wray, J., Liu, J., Nickoloff, J. A. & Shen, Z. Distinct RAD51 Associations with
540 RAD52 and BCCIP in Response to DNA Damage and Replication Stress. *Cancer*
541 *Research* **68,** 2699–2707 (2008).
542 28. Kelso, A. A. *et al.* The β-isoform of BCCIP promotes ADP release from the RAD51
543 presynaptic filament and enhances homologous DNA pairing. *Nucleic Acids*
544 *Research* **45,** 711–725 (2017).
545 29. Moldovan, G.-L. & D'Andrea, A. D. How the fanconi anemia pathway guards the
546 genome. *Annu. Rev. Genet.* **43,** 223–249 (2009).
547 30. Taylor, R. M., Moore, D. J., Whitehouse, J., Johnson, P. & Caldecott, K. W. A cell
548 cycle-specific requirement for the XRCC1 BRCT II domain during mammalian
549 DNA strand break repair. *Mol Cell Biol* **20,** 735–740 (2000).
550 31. Dutta, A. *et al.* Microhomology-mediated end joining is activated in irradiated
551 human cells due to phosphorylation-dependent formation of the XRCC1 repair
552 complex. *Nucleic Acids Research* **45,** 2585–2599 (2017).
553 32. Critchlow, S. E., Bowater, R. P. & Jackson, S. P. Mammalian DNA double-strand
554 break repair protein XRCC4 interacts with DNA ligase IV. *Curr Biol* **7,** 588–598
555 (1997).
556 33. Normanno, D. *et al.* Mutational phospho-mimicry reveals a regulatory role for the
557 XRCC4 and XLF C-terminal tails in modulating DNA bridging during classical
558 non-homologous end joining. *eLife* **6,** 1093 (2017).
559 34. Sehorn, M. G., Sigurdsson, S., Bussen, W., Unger, V. M. & Sung, P. Human meiotic
560 recombinase Dmc1 promotes ATP-dependent homologous DNA strand exchange.
561 *Nature* **429,** 433–437 (2004).
562 35. Wang, A. T. *et al.* A Dominant Mutation in Human RAD51 Reveals Its Function in
563 DNA Interstrand Crosslink Repair Independent of Homologous Recombination.
564 *Mol. Cell* **59,** 478–490 (2015).
565 36. Zadorozhny, K. *et al.* Fanconi-Anemia-Associated Mutations Destabilize RAD51
566 Filaments and Impair Replication Fork Protection. *Cell Reports* **21,** 333–340 (2017).
567 37. Yu, D. S. *et al.* Dynamic control of Rad51 recombinase by self-association and
568 interaction with BRCA2. *Mol. Cell* **12,** 1029–1041 (2003).
569 38. Marsden, C. G. *et al.* The Tumor-Associated Variant RAD51 G151D Induces a
570 Hyper-Recombination Phenotype. *PLoS Genet* **12,** e1006208 (2016).
571 39. Deng, Q., Ramsköld, D., Reinius, B. & Sandberg, R. Single-cell RNA-seq reveals
572 dynamic, random monoallelic gene expression in mammalian cells. *Science* **343,**
573 193–196 (2014).
574 40. Chen, J. *et al.* Tumor-associated mutations in a conserved structural motif alter
575 physical and biochemical properties of human RAD51 recombinase. *Nucleic Acids*
576 *Research* **43,** 1098–1111 (2015).
577 41. Hammond, A. M. *et al.* The creation and selection of mutations resistant to a gene
578 drive over multiple generations in the malaria mosquito. *PLoS Genet* **13,** e1007039
579 (2017).
580 42. Champer, J. *et al.* Reducing resistance allele formation in CRISPR gene drive.
581 *Proceedings of the National Academy of Sciences* **115,** 5522–5527 (2018).

43. Santos, F. *et al.* Active demethylation in mouse zygotes involves cytosine deamination and base excision repair. *Epigenetics & Chromatin* **6,** 39 (2013).
44. Schindelin, J. *et al.* Fiji: an open-source platform for biological-image analysis. *Nat Meth* **9,** 676–682 (2012).

Supplementary Information

Additional data and sequences of oligos, proteins, and primers used in this study can be found in Supplementary Information.

Acknowledgements

The experiments described in this manuscript were funded by the Tan-Yang Center for Autism Research at MIT and the Poitras Center for Affective Disorders Research at MIT. We would like to thank Tetsushi Sakuma and Takashi Yamamoto of Hiroshima University for sharing their knock-in enhancer screening data. We would also like to thank Ricardo del Rosario for assistance with analysis of published single-cell RNA-seq data. Finally, we are grateful for the helpful discussion and insight provided by Charles Jennings, Sabbi Lall, and members of the Feng lab.

Author Contributions

J.J.W., T.A., M.W., Q.Z., and G.F. designed experiments. J.J.W. and P.Q. performed experiments. J.J.W., T.A., M.W., and G.F. analyzed data. J.J.W., T.A., and G.F. prepared the manuscript.

Reprints

Reprints and permission information is available at www.nature.com/reprints.

Competing Financial Interests

MIT and J.J.W, T.A., M.W., Q.Z. and G.F. have submitted a provisional patent application (U.S. Provisional Application No.: 62/623,006) related to the use of enhanced interhomolog repair for

611 gene editing purposes.

612 **Materials and Correspondence**

613 Correspondence and requests for materials should be addressed to G.F. at fengg@mit.edu

614

615

616

617

618

619

620

621

622

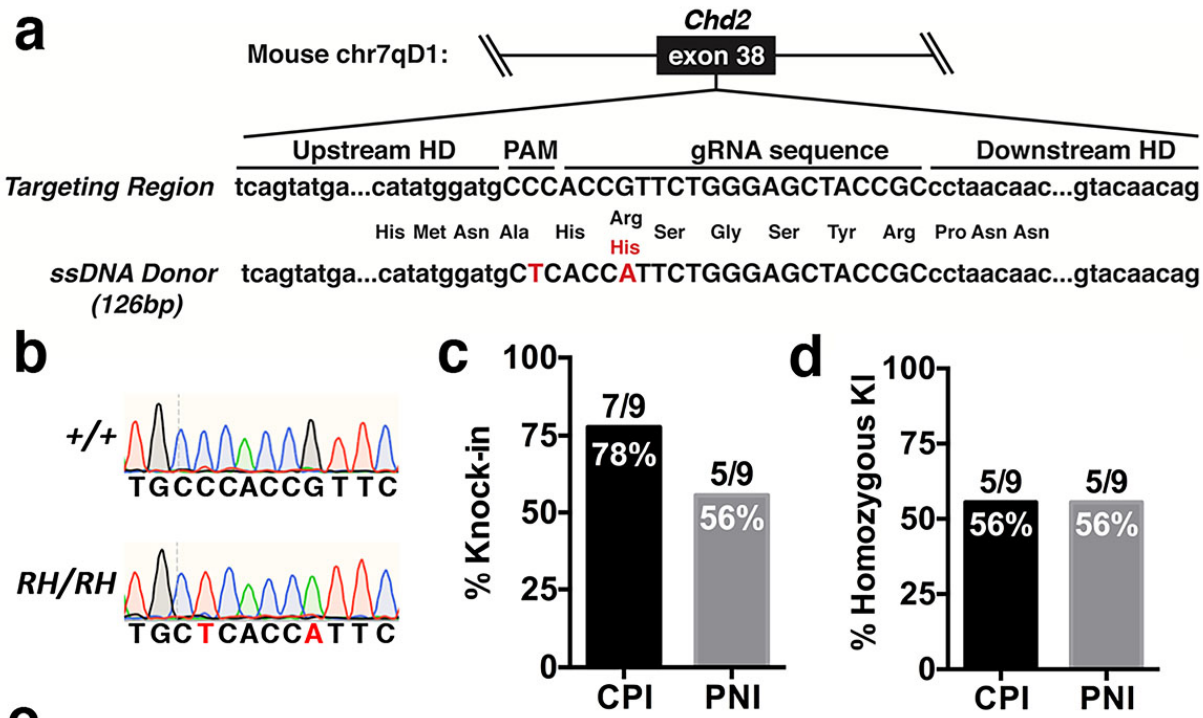

e

Injection Method	Father ID (Genotype)	Mother ID (Genotype)	F_1 Het Pups
CPI	C57BL/6N (+/+)	9989 (*RH/RH*)	8/8
CPI	C57BL/6N (+/+)	9991 (*RH/RH*)	4/4
PNI	C57BL/6N (+/+)	9995 (*RH/RH*)	6/6
CPI	9992 (*RH/RH*)	C57BL/6N (+/+)	6/6
CPI	9994 (*RH/RH*)	C57BL/6N (+/+)	9/9
PNI	10000 (*RH/RH*)	C57BL/6N (+/+)	3/3

Figure 1 | Efficient homozygous knock-in with RAD51. a, Schematic of the targeting locus and HR donor for generating *Chd2*^{R1684H} mutant mice. HR donor contains both the c.5051G>A point mutation and a synonymous mutation that destroys the relevant PAM site (HD=homology domain). **b,** Example chromatograms of wildtype (top) and *Chd2*$^{R1684H/R1684H}$ animals (RH=R1684H). **c,** Overall KI efficiency observed in F_0 pups derived from either cytoplasmic (CPI) or pronuclear (PNI) injection (pups with ≥1 KI allele/total pups). **d,** Homozygous KI rates observed in F_0 pups generated by either CPI or PNI. **e,** Genotyping results from F_1 pups derived from crosses between F_0 *Chd2*$^{R1684H/R1684H}$ animals and wildtype C57BL/6N animals.

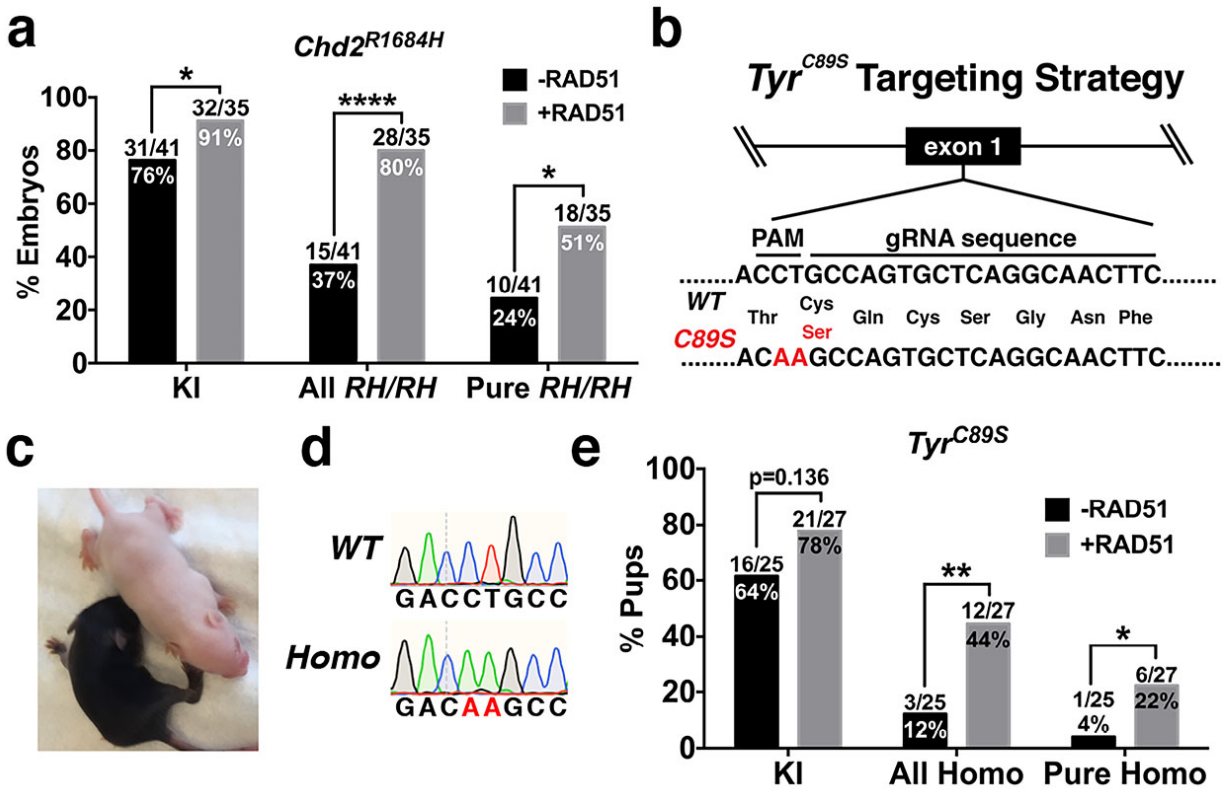

Figure 2 | RAD51 enhances homozygous KI efficiency at multiple loci. a, Quantification of KI efficiency (left) and homozygous KI efficiency in embryos generated by *Chd2*^{R1684H} PNI with or without RAD51. All *RH/RH* includes mosaic embryos and denotes embryos with >2:1 ratio of mutant allele to wildtype allele (KI: p=0.034, one-tailed chi-square test; All *RH/RH*: p<0.0001, one-tailed chi-square test; Pure *RH/RH*: p=0.015, one-tailed chi-square test). **b,** Schematic of knock-in strategy for the albinism-associated *Tyr*^{C89S} mutation. **c,** Representative examples of *Tyr*$^{+/+}$ (black) and *Tyr*$^{C89S/C89S}$ (white) littermates derived from three-component CRISPR injections using exogenous RAD51 protein. **d,** Representative chromatograms from *Tyr*$^{+/+}$ (top) and *Tyr*$^{C89S/C89S}$ animals. **e,** Genotyping of F_0 animals generated by three-component CRISPR targeting the *Tyr*^{C89S} locus with or without RAD51 (KI: p=0.136, one-tailed chi-square test; All Homo: p=0.0081, one-tailed chi-square test; Pure Homo: p=0.0272, one-tailed chi-square test).

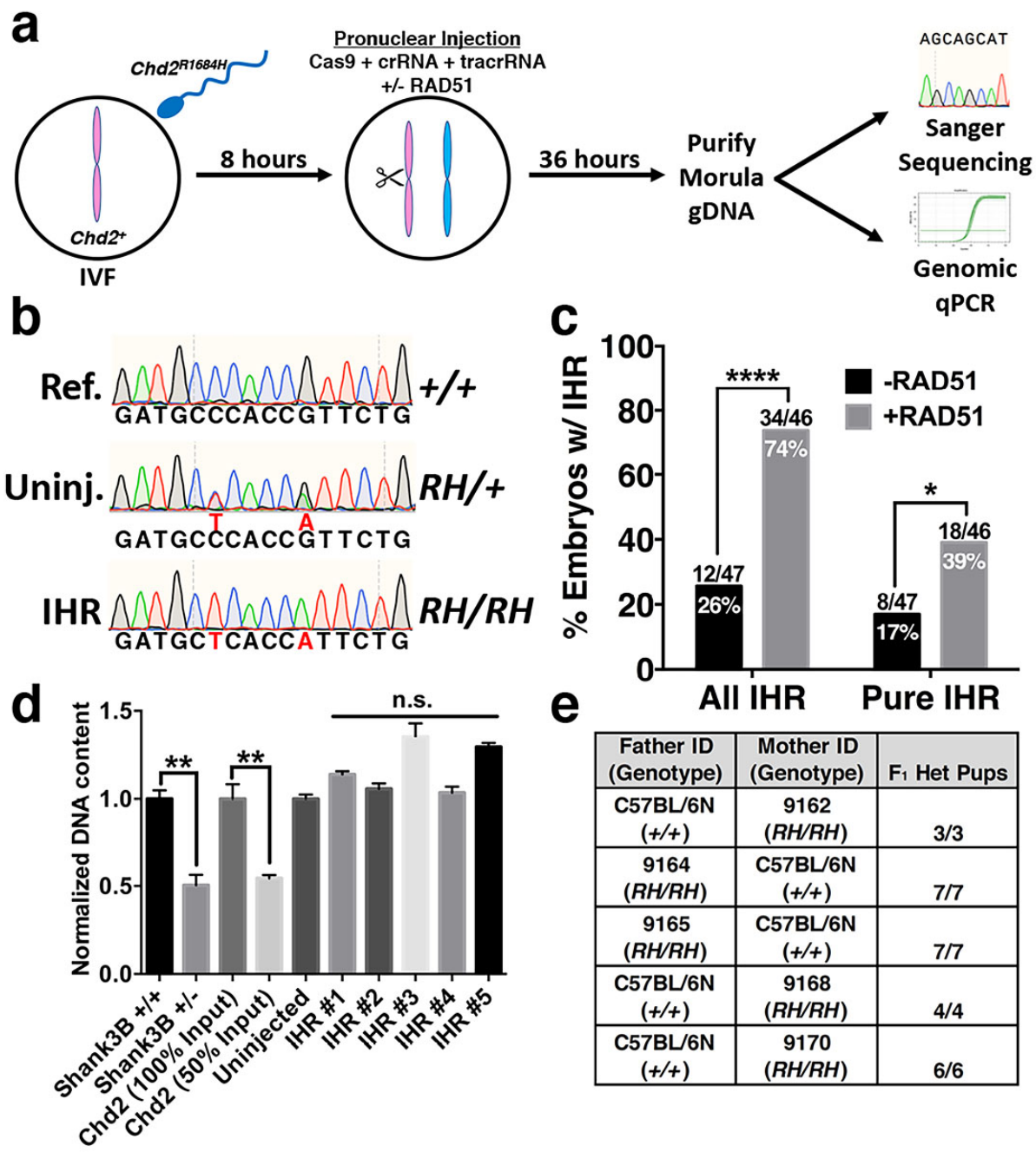

Father ID (Genotype)	Mother ID (Genotype)	F_1 Het Pups
C57BL/6N (+/+)	9162 (*RH/RH*)	3/3
9164 (*RH/RH*)	C57BL/6N (+/+)	7/7
9165 (*RH/RH*)	C57BL/6N (+/+)	7/7
C57BL/6N (+/+)	9168 (*RH/RH*)	4/4
C57BL/6N (+/+)	9170 (*RH/RH*)	6/6

Figure 3 | RAD51 enhances interhomolog repair. a, Schematic of strategy for testing RAD51-enhanced IHR. Wildtype C57BL/6N eggs were fertilized *in vitro* by sperm collected from male *Chd2*$^{R1684H/R1684H}$ mice and cultured for 8 hours. At 8hpf, PNI was performed with Cas9 protein, crRNA, and tracrRNA with or without RAD51 protein. Since *R1684H* mutants carry a mutation in the PAM associated with the crRNA utilized in these experiments, Cas9 is only capable of cutting the maternal allele. Injected embryos were then cultured for 48 hours and collected at morula stage. Half of the purified DNA was used for nested PCR and Sanger sequencing and the

653 other half was used for multiplex PCR and subsequent qPCR to analyze genomic copy number at
654 the *Chd2* editing locus. **b,** Representative chromatograms showing the wildtype reference
655 sequence (Ref., top), an uninjected *Chd2*$^{R1684H/+}$ embryo generated by IVF (Uninj., middle), and
656 a pure *Chd2*$^{R1684H/R1684H}$ homozygous mutant (IHR, bottom) generated via donor-free, RAD51-
657 enhanced three-component CRISPR. **c,** Quantification of Sanger sequencing results from IVF-
658 derived embryos co-injected with or without RAD51. 'All IHR' includes mosaic embryos and
659 was determined by identifying embryos with >2:1 ratio of R1684H-to-wildtype alleles (one-
660 tailed chi-square test, $p<0.0001$). Pure IHR refers to embryos without mosaicism ($p=0.018$, one-
661 tailed chi-square test). **d,** Genomic qPCR targeting *Shank3B* using 180pg genomic DNA from
662 wildtype and *Shank3B*$^{+/-}$ mice as a control for copy-number sensitivity (lanes 1-2, $p=0.00295$,
663 unpaired t-test, $t=6.47$, $df=4$, $n=3$ technical replicates per sample, error bars=SEM). Lanes 3-4
664 illustrate genomic qPCR for the *Chd2*^{R1684H} locus using 100% and 50% input of DNA derived
665 from wildtype blastocysts for *Chd2* quantification (but 100% input for *Gapdh*) as a control for
666 copy-number sensitivity at the locus ($p=0.0099$, unpaired t-test, $t=5.355$, $df=3.302$, $n=4$ technical
667 replicates per condition, error bars=SEM). Lanes 5-10 illustrate genomic qPCR for the
668 *Chd2*^{R1684H} locus using DNA from an uninjected embryo and 5 randomly selected pure
669 homozygous *Chd2*^{R1684H} embryos ($p>0.05$, unpaired t-test, $t=4.60$, $df=6$, $n=4$ technical replicates
670 per sample, error bars=SEM)**. e,** F_1 genotyping results of litters derived from crosses between
671 wildtype C57BL/6N mice and 5 pure *Chd2*$^{R1684H/R1684H}$ F_0 animals generated by IVF with
672 RAD51.

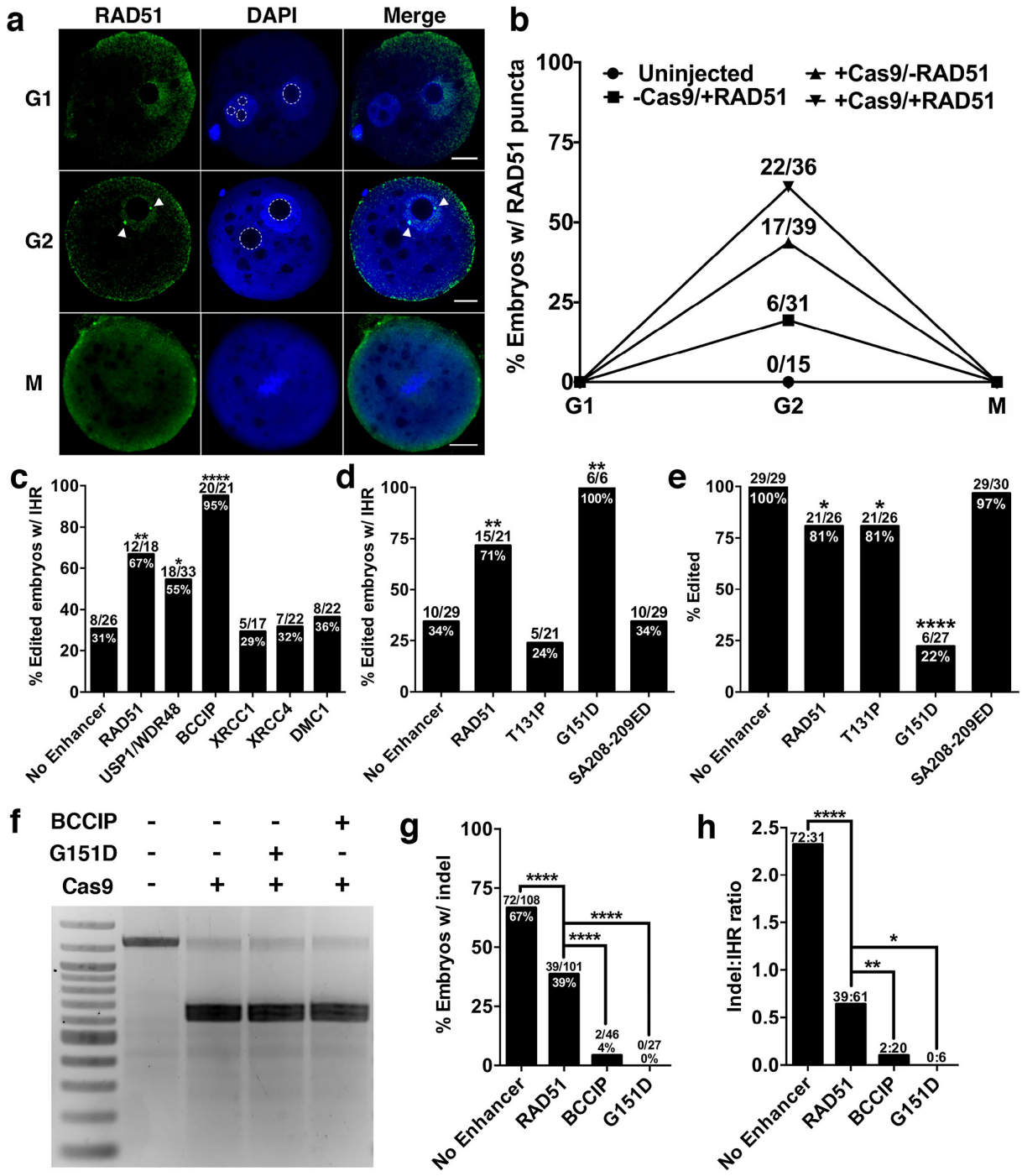

Figure 4 | RAD51 G151D and BCCIP promote zygotic IHR and suppress indel formation. **a,** Representative images of RAD51 immunostaining from Cas9 + RAD51-injected embryos during G1, G2, and M-phase. Arrowheads indicate RAD51 puncta. Dotted lines highlight pronuclear nucleoli. **b,** Quantification of immunocytochemistry for RAD51 displaying the number of zygotes positive for RAD51 puncta during G1, G2, or M-phase. **c,** Quantification of

679 IHR efficiency based on *Chd2*^{R1684H} genotyping of blastocysts derived from embryos injected
680 with Cas9/crRNA/tracrRNA and the indicated DSB repair-related proteins. Quantification
681 includes mosaic embryos (one-tailed chi-square test). **d,** Quantification of IHR efficiency in
682 blastocysts derived from Cas9/crRNA/tracrRNA-injected embryos co-injected with the indicated
683 RAD51 variants (one-tailed chi-square test). **e,** Quantification of editing efficiency at the
684 *Chd2*^{R1684H} locus in embryos injected with Cas9/crRNA/tracrRNA and the indicated RAD51
685 variants (one-tailed chi-square test). **f,** *In vitro* Cas9 nuclease activity assay using a PCR
686 amplimer of the *Chd2*^{R1684H} locus and Cas9 alone or co-incubated with either RAD51 G151D or
687 BCCIP. **g,** Quantification of the percent of total injected embryos carrying an indel after injection
688 with the specified proteins. **h,** Quantification of the ratio of indel-positive embryos to IHR-
689 positive embryos derived from injections with the specified proteins.
690
691
692
693
694
695
696
697
698
699
700
701
702
703
704
705
706
707
708
709

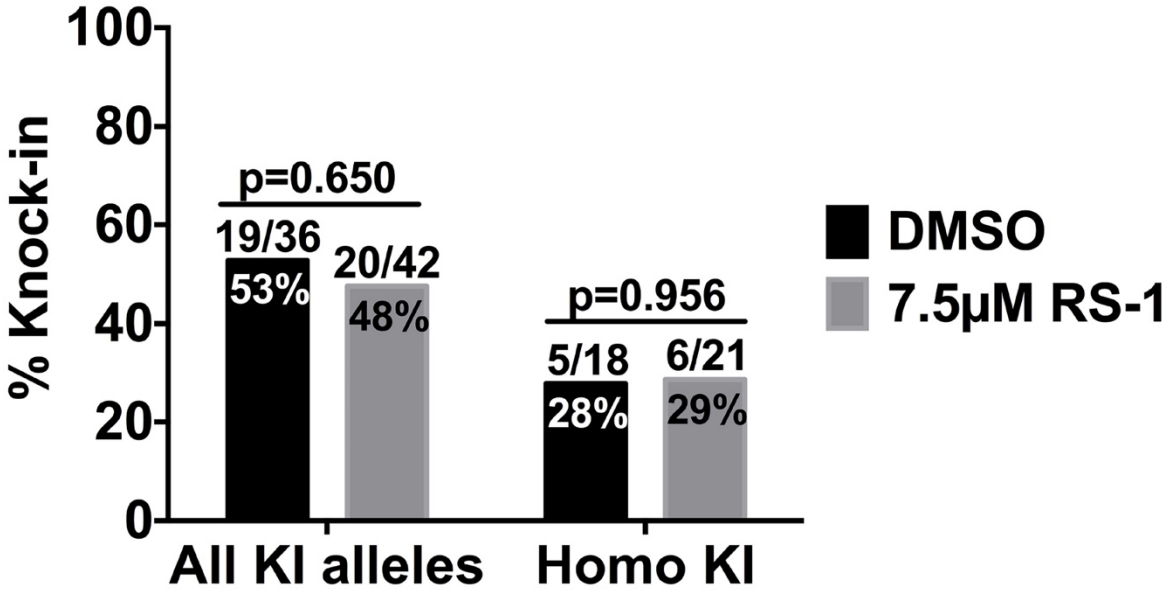

Extended Data Figure 1 | RS-1 does not alter KI efficiency with ssODNs in mouse zygotes. *Chd2*^{R1684H} KI and homozygous KI efficiency in embryos cultured in either DMSO or 7.5μM RS-1 for 24 hours (two-tailed chi-square test).

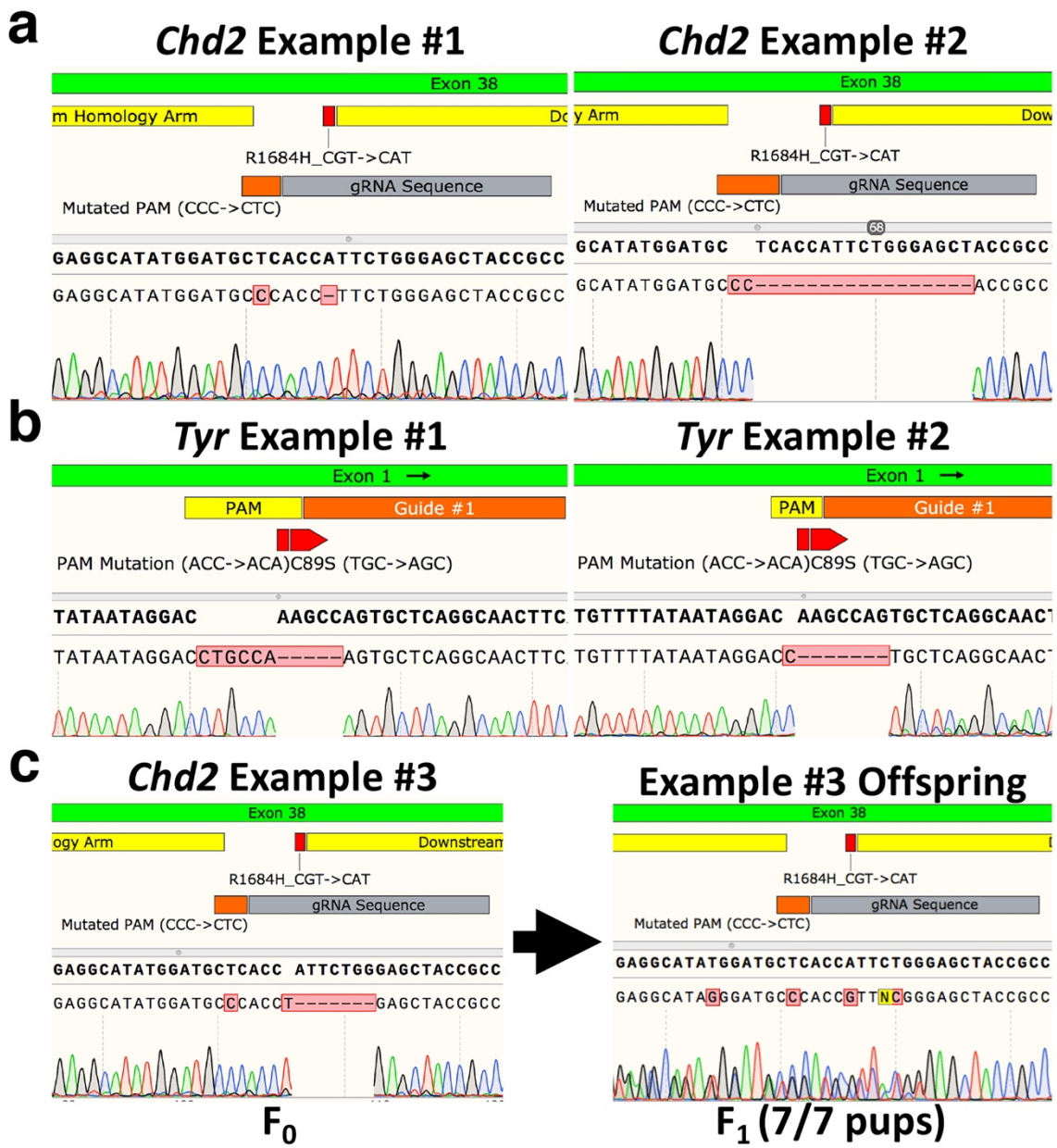

Extended Data Figure 2 | RAD51 stimulates the generation of homozygous indels. a, Representative Sanger sequencing traces of putative homozygous indels observed in F_0 animals obtained from *Chd2*^{R1684H} knock-in experiments. **b,** Representative Sanger sequencing traces of putative homozygous indels observed in F_0 animals obtained from *Tyr*^{C89S} knock-in experiments. **c,** Genotyping traces for a putative homozygous *Chd2* indel and an F_1 offspring from a cross between the founder and a wildtype C57BL/6N mate. The F_1 genotyping, which was consistent for all 7 pups in the litter, indicates heterozygous presence of the indel observed in the founder.

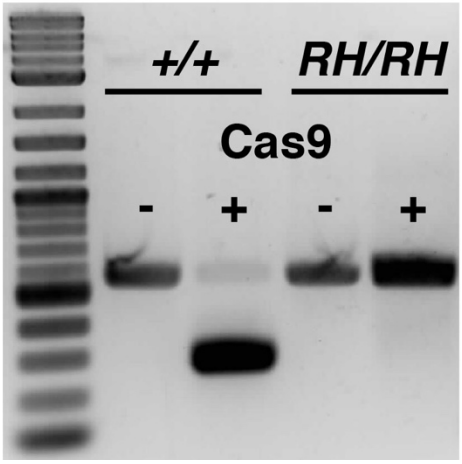

Extended Data Figure 3 | *Chd2* crRNA specifically recognizes wildtype allele. PCR was performed using the Chd2-RH_F/R primer pair with DNA purified from either wildtype or *Chd2*$^{R1684H/R1684H}$ mice and the PCR product was used as a template for *in vitro* digestion assays with or without Cas9.

787

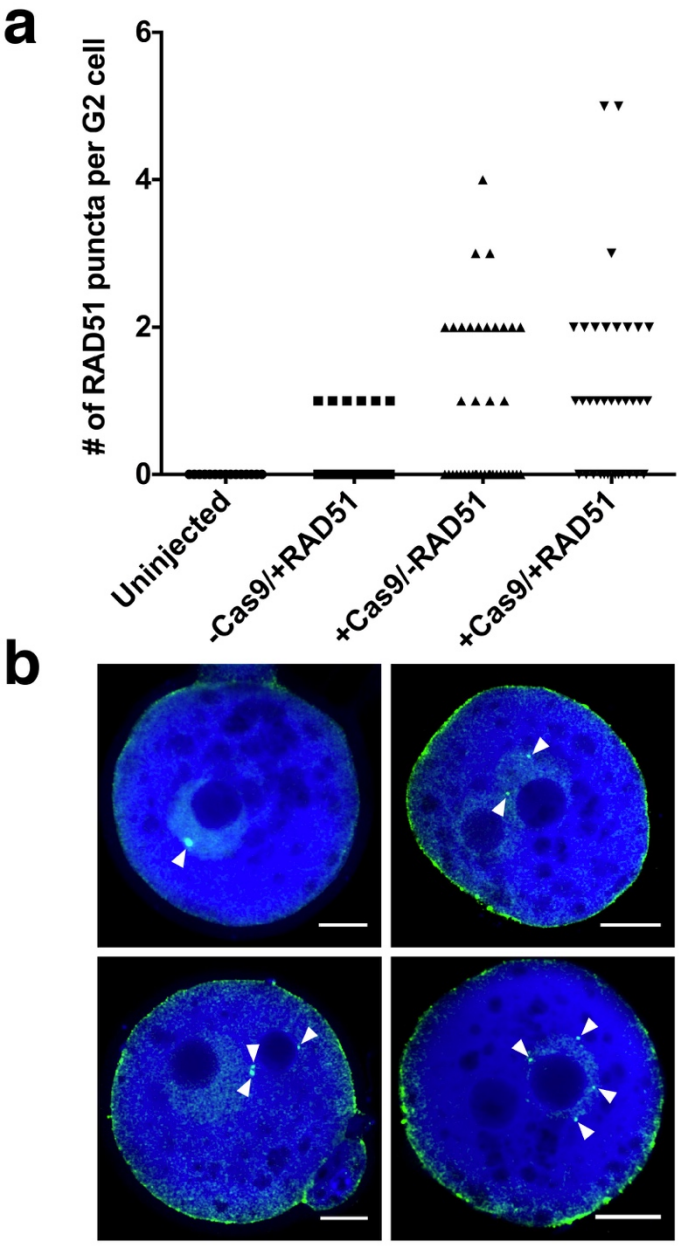

788
789
790 **Extended Data Figure 4 | Cas9 injection alters the number of RAD51 puncta in G2. a,**
791 Quantification of RAD51 puncta number observed in control G2 zygotes and cells injected with
792 RAD51 alone, Cas9/crRNA/tracrRNA alone, or Cas9/crRNA/tracrRNA and RAD51. Each point
793 represents a single cell. **b,** Representative images of cells with one (top left), two (top right),
794 three (bottom left), or four (bottom right) RAD51 puncta (arrowheads indicate puncta; DAPI,
795 blue; RAD51, green; scale=10μm).
796
797
798
799
800

801
802

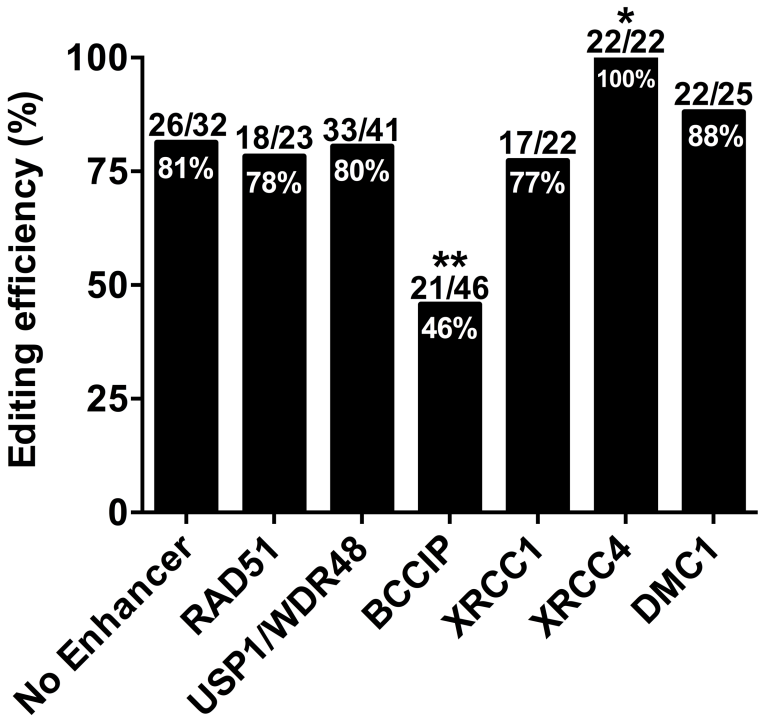

803
804 **Extended Data Figure 5 | Decreased editing efficiency in BCCIP-injected cells.** Editing
805 efficiency observed in IVF-derived embryos injected with Cas9/crRNA/tracrRNA only (no
806 enhancer) or the indicated HR- and DSB repair-associated proteins (BCCIP: p=0.0016, two-
807 tailed chi-square test; XRCC4: p=0.031, two-tailed chi-square test).
808
809
810
811
812
813
814
815
816

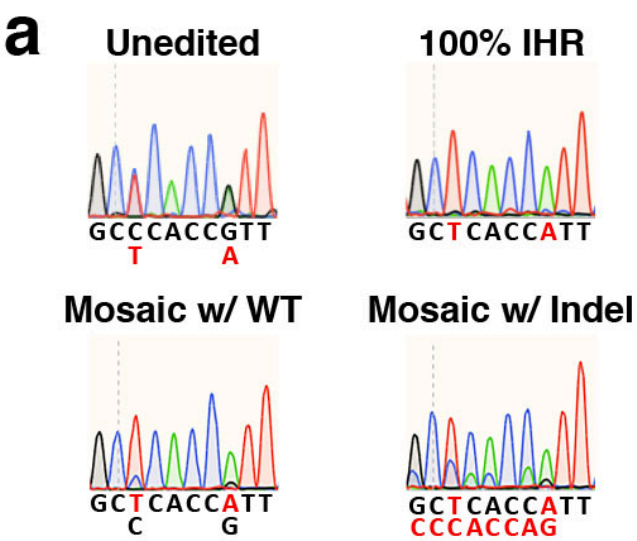

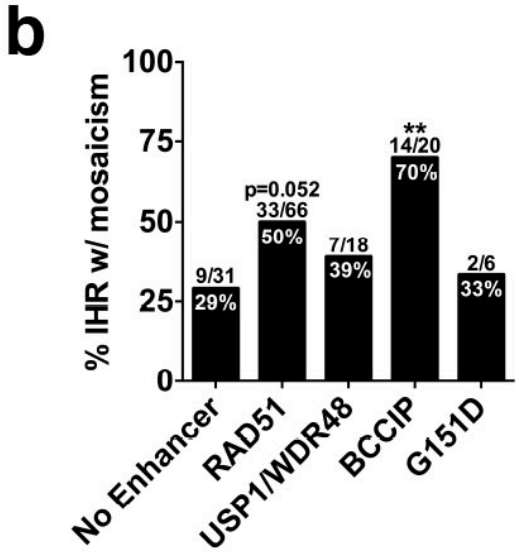

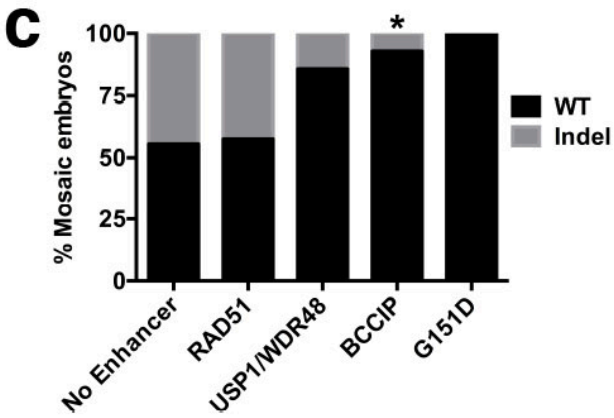

d

Condition	# Mosaic w/ WT	# Mosaic w/ Indel
No Enhancer	5	4
RAD51	19	14
G151D	2	0
USP1/WDR48	6	1
BCCIP	13	1

Extended Data Figure 6 | Effects of IHR enhancers on mosaicism. a, Representative chromatograms showing examples traces for genotypes characterized as unedited (top left), 100% IHR (top right), mosaic with wildtype (bottom left), and mosaic with indel (bottom right). **b,** Quantification of mosaicism in embryos displaying IHR for all conditions analyzed. Data includes all IVF-derived embryos **(Figs. 3c**, **4c**, and **4d**; BCCIP: p=0.0041, two-tailed chi-square test). **c,** Distribution of types of mosaicism observed in mosaic embryos described in panel b (BCCIP: p=0.034, two-tailed chi-square test). **d,** Numbers for observed mosaicism used to generate panel **c**.

834

Sex	Injection Method	Genotype	Notes
Female	CPI	RH/RH	
Female	CPI	RH/Indel	
Female	CPI	RH/RH	
Male	CPI	RH/RH	
Male	CPI	RH/RH	
Female	CPI	Indel/Indel	Same Indel
Female	CPI	RH/Indel	
Female	CPI	RH/RH	
Male	CPI	Indel/Indel	Different Indels
Female	PNI	RH/RH	
Male	PNI	RH/RH	
Male	PNI	RH/RH	
Female	PNI	Indel/Indel	Different Indels
Male	PNI	Indel/Indel	Same Indel
Male	PNI	RH/RH	
Male	PNI	Indel/Indel	Same Indel
Female	PNI	Indel/Indel	Same Indel
Female	PNI	RH/RH	

835

836 **Extended Data Table 1 | Genotyping Results for Individual F_0 Pups from CPI and PNI**
837 **Experiments in Figure 1**. Genotyping was performed using the C2RH-Long_F1/R1 primer pair
838 described in Supplementary Table 3.
839
840
841
842
843
844
845
846
847
848
849
850
851

852

Condition	Coat Color	Genotype
-RAD51	White	C89S/C89S
-RAD51	White	C89S/Indel
-RAD51	White	C89S/Indel
-RAD51	White	C89S/Indel
-RAD51	White	C89S/Indel
-RAD51	White	C89S/Indel
-RAD51	White	C89S/Indel
-RAD51	White	Indel/Indel (Different)
-RAD51	White	Indel/Indel (Different)
-RAD51	White	Indel/Indel (Different)
-RAD51	White	Indel/Indel (Different)
-RAD51	Mixed	C89S/C89S
-RAD51	Mixed	C89S/C89S
-RAD51	Mixed	C89S/Indel
-RAD51	Mixed	C89S/Indel
-RAD51	Mixed	C89S/Indel
-RAD51	Mixed	C89S/Indel
-RAD51	Mixed	C89S/Indel
-RAD51	Mixed	Indel/Indel (Different)
-RAD51	Mixed	Indel/Indel (Different)
-RAD51	Mixed	Indel/Indel (Different)
-RAD51	Black	C89S/+
-RAD51	Black	C89S/+
-RAD51	Black	Indel/+
-RAD51	Black	Indel/+
+RAD51	White	C89S/C89S
+RAD51	White	C89S/C89S
+RAD51	White	C89S/C89S
+RAD51	White	C89S/C89S
+RAD51	White	C89S/C89S
+RAD51	White	C89S/C89S
+RAD51	White	C89S/Indel
+RAD51	White	C89S/Indel
+RAD51	White	C89S/Indel
+RAD51	White	Indel/Indel (Same)
+RAD51	Mixed	C89S/C89S
+RAD51	Mixed	C89S/C89S
+RAD51	Mixed	C89S/C89S
+RAD51	Mixed	C89S/C89S
+RAD51	Mixed	C89S/C89S
+RAD51	Mixed	C89S/C89S
+RAD51	Mixed	C89S/Indel
+RAD51	Mixed	C89S/Indel
+RAD51	Mixed	C89S/Indel
+RAD51	Mixed	Indel/Indel (Different)
+RAD51	Mixed	Indel/Indel (Same)
+RAD51	Black	C89S/+
+RAD51	Black	C89S/+
+RAD51	Black	C89S/+
+RAD51	Black	Indel/+
+RAD51	Black	Indel/+
+RAD51	Black	Indel/+

853

854 **Extended Data Table 2 | Genotype-phenotype analyses of Tyr^{C89S} pups from Figure 2b-e.**
855 Phenotype analysis (coat color) and corresponding genotyping data from genomic DNA purified
856 from albino tissue (if available).
857
858
859
860
861
862
863
864
865
866

867

Condition	Positive	Negative	Total	p-Value vs. Uninjected	p-Value vs. RAD51-only	p-Value vs. Cas9-only	p-Value vs. Cas9 + RAD51
Uninjected	0	15	15	N/A	0.0677	0.002	<0.0001
RAD51-only	6	25	31	0.0677	N/A	0.016	0.0003
Cas9-only	17	22	39	0.002	0.016	N/A	0.0646
Cas9 + RAD51	22	14	36	<0.0001	0.0003	0.0646	N/A

868

869 **Extended Data Table 3 | Chi-square analyses of immunocytochemistry data from Figure**
870 **4b.**
871